Impact of interface structure on magnetic exchange coupling in MnBi/Fe_xCo_{1-x} bilayers

S. Sabet,[1,*] A. Moradabadi,[1,2] S. Gorji,[3,4] M. Yi,[1] Q. Gong,[1] M. H. Fawey,[3,4] E. Hildebrandt,[1] D. Wang,[3,5] H. Zhang,[1] B.-X. Xu,[1] C. Kübel,[3,5] and L. Alff[1,†]

[1]*Institute of Materials Science, Technische Universität Darmstadt, 64287 Darmstadt, Germany*

[2]*Institut für Chemie und Biochemie, Freie Universität Berlin, 14195 Berlin, Germany*

[3]*Institute of Nanotechnology (INT), Karlsruhe Institute of Technology (KIT), 76344 Eggenstein-Leopoldshafen, Germany*

[4]*Joint Research Laboratory Nanomaterials (KIT and TUD) at Technische Universität Darmstadt, Jovanka-Bontschits-Strasse 2, 64287 Darmstadt, Germany*

[5]*Karlsruhe Nano Micro Facility, Karlsruhe Institute of Technology (KIT), 76344 Eggenstein-Leopoldshafen, Germany*

(Received 10 May 2018; revised manuscript received 3 October 2018; published 29 November 2018)

Magnetic exchange coupling behavior was investigated in MnBi/FeCo bilayer system at the hard/soft magnetic interface. We performed a combined study of cross-sectional high resolution transmission electron microscopy (HR-TEM), DFT calculations, and micromagnetic simulations to elucidate effect of interface structure on exchange coupling. Exchange spring MnBi/Fe_xCo_{1-x} ($x = 0.65$ and 0.35) bilayers with various thicknesses of the soft magnetic layer were deposited in a dc magnetron sputtering unit from alloy targets. According to magnetic measurements, using a Co-rich layer leads to a more coherent exchange coupling with optimum soft layer thickness of about 1 nm. Our DFT calculations predicted formation of a polycrystalline FeCo layer with coexisting crystalline and disordered (110) phases. The indexed FFTs from HR-TEM images confirmed a crystalline FeCo(110) layer, with slight misorientation in some areas, and a disordered region close to the interface which deteriorates interface exchange coupling. Moreover, our micromagnetic simulations showed how the thickness of the FeCo layer and the interface roughness both control the effectiveness of exchange coupling in MnBi/FeCo bilayer.

DOI: 10.1103/PhysRevB.98.174440

I. INTRODUCTION

Exchange spring magnets provide an interesting approach to enable synthesis of rare-earth free permanent magnets with comparable magnetic properties to commercialized rare-earth based magnets [1–3]. In order to be qualified as replacements for rare-earth magnets, it is required that new candidates have high magnetic anisotropy, high energy product, and high temperature stability [4]. The low temperature phase (LTP) of MnBi is one of the candidates with a particularly high intrinsic magnetic anisotropy on the order of 10^7 erg/cm^3 (1 MJ/m^3) as well as a large coercivity (about 1.6 T), which rather uniquely shows a positive temperature coefficient [5–7]. Moreover, the relatively high Curie temperature of 630 K also makes MnBi an interesting material for high temperature applications [8]. However, in spite of such extraordinary magnetic properties, the main drawback of MnBi for permanent magnet application is its comparably low saturation magnetization of 710 emu/cm^3 (0.71 MA/m) limiting the maximum achievable energy product [6].

As suggested back in 1991 by Kneller and Hawig, one way to overcome this barrier and further improve the energy product is through the synthesis of exchange spring magnets with coupled hard/soft magnetic phases [9–15]. Such composite magnets, e.g., coupled bilayers of MnBi in combination with FeCo as the soft phase, will possess a much higher saturation magnetization and thus an increased overall energy product (for a schematic of a two-phase exchange spring magnet see the Supplemental Material) [16]. The total magnetization in such a bilayer is given by the volume average of magnetization in the hard and soft magnetic layers [11,14].

Based on the model suggested by Kneller [9], there is a critical thickness (volume) of soft magnetic phase which is limited by the domain wall width (or exchange length) of the hard magnetic phase [11,12]. This model suggests that only for a soft magnetic layer thickness less than twice of the domain wall width for the hard magnetic phase, the bilayer is expected to behave as a single hard phase with increased magnetization in which both soft and hard phases switch coherently during magnetic reversal under opposing fields ($H < 0$).

Experimentally, even for sufficiently thin soft magnetic layers incomplete exchange coupling is observed in the previously reported hysteresis loops, i.e., less rectangular hysteresis shape and a shoulder at zero field during magnetic reversal process [17–20]. The incoherent hysteresis loops with decreased energy product in hard/soft exchange coupled layers can result from the weak interface exchange caused by interface structure, or inhomogeneities [21]. According to the results of a few available studies on MnBi exchange spring bilayers, the coupling between the MnBi and Fe_xCo_{1-x} layers is incoherent for soft magnetic layers thicker than ~4 nm [17–20]. Based on their calculations, Gao *et al.* have also argued that the formation of a Co-rich Fe_xCo_{1-x} layer at the

*sabet@oxide.tu-darmstadt.de
†alff@oxide.tu-darmstadt.de

interface with MnBi is beneficial for exchange coupling where according to their experimental data the strongest coupling occurs in MnBi/Co bilayers with an optimum Co thickness of ∼3 nm [17]. Therefore, it is important to understand the interfacial features responsible for an incoherent interlayer exchange coupling in order to make further advances for effectiveness of exchange spring magnets.

In this work we combined theoretical and experimental methods to study the exchange coupling behavior in the MnBi/FeCo bilayer system, focusing on the interface structural factors including the effect of degree of crystallinity, interface roughness, and composition of the soft magnetic phase. Our aim is to identify which of these factors mainly control the strength of exchange coupling in the MnBi/FeCo system.

II. EXPERIMENTAL AND THEORETICAL PROCEDURE

Exchange coupled bilayers of MnBi/FeCo have been deposited onto quartz glass substrates in a dc magnetron sputtering system. The structure and composition of the bilayer samples have been analyzed using XRD and HR-TEM equipped with EDX. The magnetic measurements have been performed using a SQUID magnetometer. To simulate the hard/soft interface and analyze the effect of structural factors on exchange properties, density functional theory (DFT) calculations using the projected augmented wave method as implemented in the Vienna *ab initio* simulation package (VASP) [22] with GGA and GGA+U approximations [23,24], as well as micromagnetic simulations within a simplified model using the object oriented micromagnetic framework (3D NIST OOMMF) codes [25], have been performed. For more details on experimental and theoretical procedure see the Supplemental Material [16].

III. RESULTS AND DISCUSSION

A. Structural and magnetic characterization

The XRD patterns collected from $Mn_{55}Bi_{45}/Fe_{35}Co_{65}$ (at. %) exchange spring bilayers with various thicknesses of Co-rich soft magnetic FeCo layer are shown in Fig. 1. The peak indexing shows hexagonal MnBi (002) and (004) peaks in agreement with space group $P63/mmc$ along with some small traces of residual bismuth resulting from annealing of the MnBi films at $T_{ann} = 365\,^{\circ}C$ (638 K). Figure 1 clearly demonstrates the formation of LTP MnBi with strong c-axis texture. As expected, because of the very low thicknesses, no peaks are observed for the FeCo layer. Comparing the intensities of the MnBi (002) and (004) peaks in bilayers samples to that of the single layer MnBi thin film, all the XRD patterns show similar peak intensities implying that the MnBi hard magnetic layer in all the bilayer samples has the same high crystalline quality.

Room-temperature out-of-plane hysteresis loops for MnBi/FeCo bilayer samples with various thicknesses and two compositions of the soft magnetic layer are shown in Figs. 2(a) and 2(b). For comparison, the out-of-plane hysteresis loop for a single layer MnBi thin film sample is also included in the same graph. As expected, by addition of 1, 2, and 3 nm FeCo layers for both Fe-rich and Co-rich

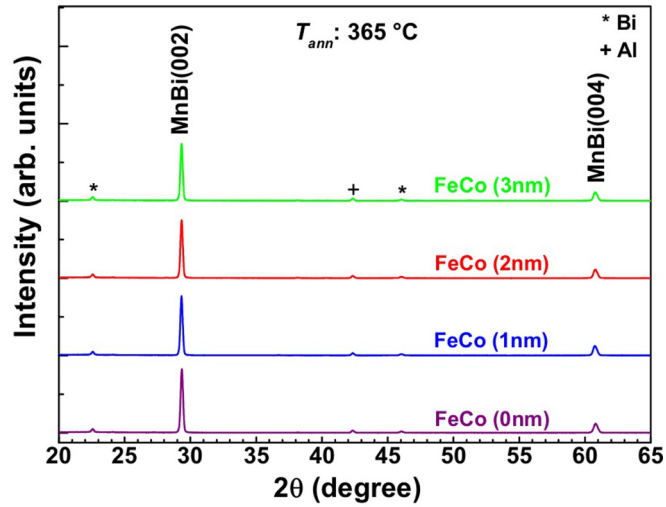

FIG. 1. The XRD patterns from exchange spring bilayers of $Mn_{55}Bi_{45}/Fe_{35}Co_{65}$ (at. %) with various thicknesses of FeCo soft magnetic layer between 1 and 3 nm. The LTP-MnBi thin films were annealed at $T_{ann} = 365\,^{\circ}C$ (638 K) followed by deposition of FeCo layer at a substrate temperature of $T_{sub} = 100\,^{\circ}C$ (373 K). The spectra have vertical offset for clarity. The peaks originating from residual bismuth in the films or Al capping layer are labeled with (*) and (+), respectively.

compositions, the saturation magnetization of exchange spring bilayer increased. According to the graphs in Fig. 2, the addition of Fe-rich soft magnetic FeCo layers improves the saturation magnetization more than the addition of Co-rich FeCo layers, since the $Fe_{65}Co_{35}$ (at. %) phase has a ∼20% larger saturation magnetization than the $Fe_{35}Co_{65}$ (at. %) phase [26]. The deposition of a 1 and 2 nm thick soft magnetic layer on top of MnBi retains the coercivity of the LTP-MnBi layer [about 15 kOe (1.5 T), even with a slight increase], while regardless of the composition of the soft magnetic layer the addition of 3 nm FeCo decreases the coercivity down to 12 kOe (1.2 T).

The exchange coupling effect between the hard and soft magnetic layers can be considered complete when the bilayer sample shows a magnetically single phase behavior. The small shoulder with an increasing slope which was observed on the measured out-of-plane hysteresis curves of the double layers during the demagnetization process around zero field indicates that the exchange coupling between the layers is incoherent. Comparing the graphs in Figs. 2(a) and 2(b) for a specific thickness, it can be seen that the observed shoulder at zero magnetic field is more significant with larger slope in the case of a Fe-rich FeCo layer showing that a Co-rich layer results in a more coherent exchange coupling.

It can be seen from the hysteresis loops in Fig. 2 that the degree of coupling decreases with increasing thickness of the soft magnetic layer and a coherent exchange coupling is only observed for a FeCo thickness of 1 nm. However, it is expected that the critical soft layer thickness above which the exchange coupling begins to deteriorate is roughly twice the domain wall width of the hard magnetic layer ($2\delta_h \simeq 2\pi\sqrt{\frac{A_h}{K_h}}$) [9,11,12] in which δ_h is the domain wall width, A_h is the exchange stiffness constant, and K_h is the magnetocrystalline

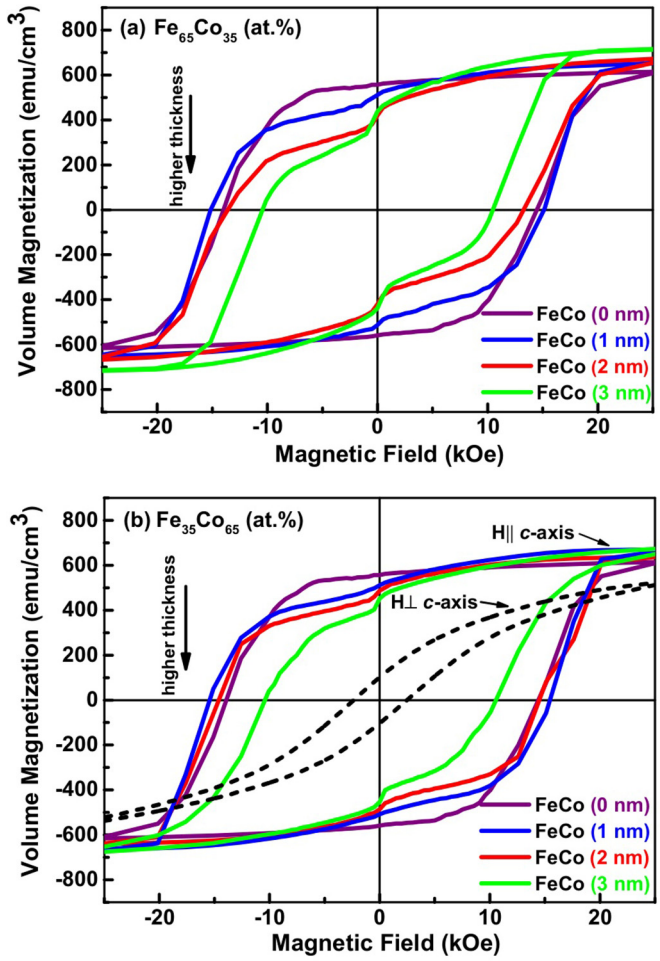

FIG. 2. Out-of-plane magnetization data for MnBi/FeCo bilayers with different FeCo thicknesses from 0 to 3 nm measured at 300 K. (a) With a Fe-rich and (b) with a Co-rich soft magnetic FeCo layer. The dashed line in (b) shows the in-plane magnetization for a single MnBi layer.

anisotropy for the hard magnetic phase. For a MnBi/FeCo bilayer with A_h and K_h equal to $\sim 8 \times 10^{-7}$ erg/cm (8 pJ/m) [27] and $\sim 1.86 \times 10^7$ erg/cm^3 (1.86 MJ/m^3) [5], respectively, the critical thickness is predicted to be as high as $\sim$13 nm. Therefore, a more detailed structural analysis of hard/soft interface is necessary to explain this lower experimentally observed critical soft layer thickness. It should also be noted that as shown in Fig. 2(b), there exists a finite in-plane component of total magnetization in the MnBi hard magnetic layer. The in-plane components of the magnetization when incompletely coupled can lead to a shoulder at the coercive field of the soft magnetic layer (H close to zero).

B. HR-TEM evaluation of MnBi/FeCo interface

To examine the interface between MnBi and FeCo, cross-sectional HR-TEM images have been captured from a MnBi/FeCo bilayer sample to investigate the crystalline structure of each layer. Moreover, the distribution of different elements across the layer was evaluated in scanning transmission electron microscopy (STEM) mode using EDX maps.

Figure 3(a) shows a cross-sectional HR-TEM image of the layers along with the fast Fourier transforms (FFTs) collected from each layer of the bilayer sample with a Co-rich soft layer. The HR-TEM image and the sharp diffraction spots in FFTs collected from the MnBi layer confirm the high crystallinity with out-of-plane orientation. The Co-rich FeCo layer, in contrary, shows a polycrystalline structure. Three different areas have been analyzed in the FeCo layer which are all crystalline, but the examined areas in the upper and lower FFTs [FFT-A1 and -A3, inset of Fig. 3(a)] are slightly misoriented. The reflections in the middle FFT pattern [FFT-A2, inset of Fig. 3(a)] in FeCo layer can be indexed as (110) lattice planes.

As it can be seen in the cross-section HR-TEM image of the MnBi/FeCo bilayer, a few atomic layers of FeCo layer grown on MnBi at the interface are disordered. This was expected since the (001) textured MnBi layer has not grown epitaxially and, in addition, FeCo and MnBi layers have different crystalline structures, i.e., hexagonal structure in MnBi and bcc structure in FeCo, and show lattice misfit which results in the growth of polycrystalline FeCo layer.

To check the elemental distribution in the bilayer sample, EDX mapping was performed on the enclosed area in Fig. 3(b). The result of the EDX mapping is consistent with the phases present in each layer. Close to the interface between the two layers the Bi concentration starts to decrease earlier than the Mn concentration, resulting in a $\approx$3 nm thick Mn-rich layer at the interface. According to the quantitative EDX analysis from this specific area on the cross section of the bilayer sample, the MnBi layer shows a stoichiometry of Mn:Bi $\sim$1.4 corresponding to a composition of $Mn_{58}Bi_{42}$ (at. %), which varies across the layer. The measured stoichiometry for the FeCo layer shows a Co:Fe ratio of $\sim$1.84, which nearly corresponds to a composition of $Fe_{35}Co_{65}$ (at. %).

C. DFT calculations of interface exchange energy: Effect of crystallinity and growth orientation

In order to shed light on the possible mechanism which affects the performance of the MnBi/FeCo exchange spring magnets, density functional theory (DFT) calculations and micromagnetic simulations (see next section) were carried out with a focus on the interface properties. Table I summarizes the result of our DFT calculations for interface formation energy (γ^{int}), interface exchange coupling energy (J^{int}) [28,29], and interface exchange constant (A^{int}) as theoretical measures to compare differences in thermodynamic stability and exchange coupling at the hard/soft interface by changing the crystalline structure and orientation.

We have calculated the above-mentioned values by modeling a MnBi (001) layer with either a crystalline or an amorphous (disordered) FeCo layer on top using VESTA code [30]. In case of a crystalline FeCo layer we have considered two different cases, one with (111) and one with (110) crystalline orientation which also show different interfacial lattice misfit with respect to MnBi layer. The amorphous structures are generated using *ab initio* molecular dynamics (AIMD) calculations from each relaxed crystalline orientation. Detailed description of DFT calculations can be found in the Supplemental Material [16].

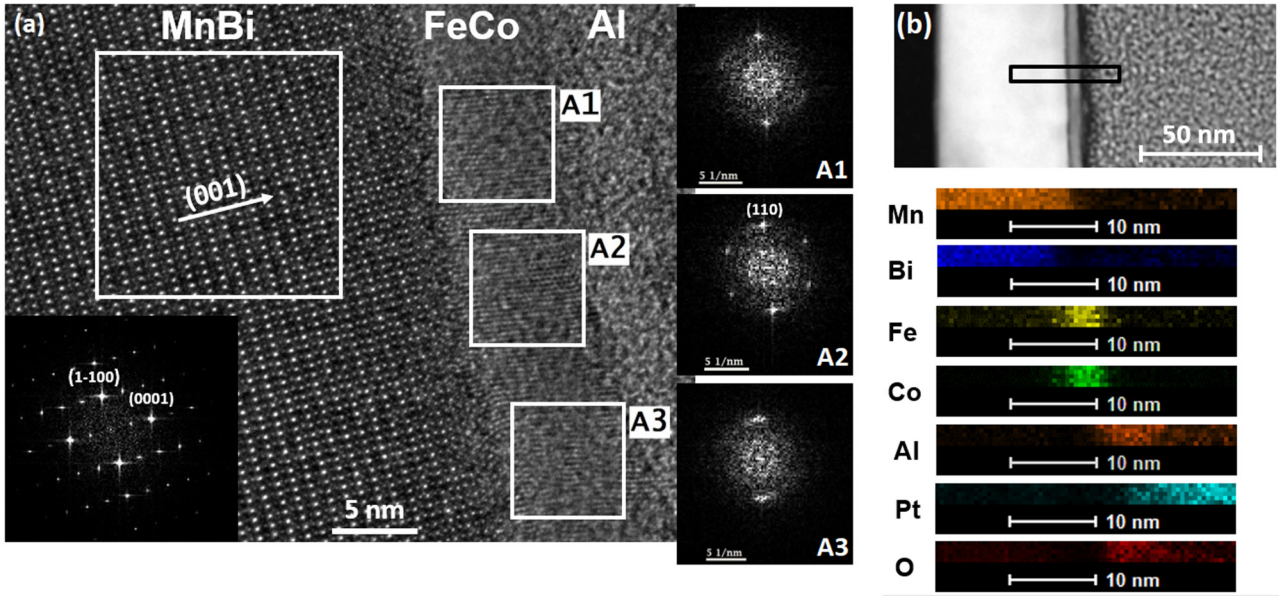

FIG. 3. (a) Cross-sectional high resolution transmission electron microscopy (HR-TEM) image from a MnBi/FeCo bilayer sample (c-axis textured MnBi hard magnetic layer with a thickness of ∼50 nm and polycrystalline Co-rich FeCo soft magnetic layer with a thickness of ∼5 nm). (b) STEM image from a cross section of the layers along with EDX elemental map from Mn, Bi, Fe, Co, Al, Pt, and O across the layers.

According to the DFT calculation results shown in Table I, the interface formation energy of the MnBi(001)/crystalline Fe_3Co_5(110) interface is lower than that of the MnBi(001)/crystalline Fe_3Co_5(111) case. This can be related to the fact that the MnBi(001)/Fe_3Co_5(110) interface has a lower lattice mismatch compared to the MnBi(001)/Fe_3Co_5(111) case and therefore is more probable to form. However, the rather similar interface formation energies (ranging from 127 to 130 meV/Å^2) suggest the possible coexistence of the crystalline (110) and disordered structures at the interface. In our cross-sectional HR-TEM image [Fig. 3(a)] at the FeCo side we also observe crystalline FeCo(110) region (with slight misorientation in some areas) along with disordered regions close to the interface which is in agreement with the result of our DFT calculations.

Moreover, it was found that in the MnBi/FeCo bilayers the most favorable atomic configuration at the interface at 0 K temperature forms with Bi termination in MnBi layer and Co termination in FeCo layer which is obtained with symmetric nonstoichiometric slab models. These findings are in agreement both with the previous study by Gao *et al.* [17] and with the cohesive energies of these elements [31]. Nevertheless, we have also modeled one case of Mn-termination in MnBi(001) layer with Co-termination in FeCo(111) layer to investigate the effect of Mn excess at the interface which resulted in slightly lower interface exchange constant (see Table I). This finding shows that the presence of Mn at the interface region does not significantly deteriorate the exchange coupling properties.

Due to higher values of J^{int} and A^{int} for the interface with crystalline Fe_3Co_5(110) compared to other configurations, its formation is in favor of a more coherent interfacial exchange coupling. However, the coexistence of disordered phases with lower values of J^{int} and A^{int} in our experimental sample can be considered as one reason for the deterioration of the magnetic exchange coupling at the hard/soft interface which results in a quasidiscontinuous magnetization in our measured hysteresis loops (see Fig. 2) [32].

D. Micromagnetic simulation of MnBi/FeCo interface: Effect of soft layer thickness and interface roughness

Since the microstructure of the experimental sample is rather complicated and cannot be fully implemented into the micromagnetic simulation, here we consider a simplified

TABLE I. Calculated values of interface formation energy γ^{int}, interface exchange coupling energy J^{int}, exchange constant A^{int}, and lattice misfit (linear and angular) obtained from DFT calculations. The disordered (110) structure is reconstructed while it lost its short-range order compared to crystalline (110) structure. The amorphous (111) is completely irregular.

Composition	Lattice misfit (longitudinal and angular)	Surface termination	Orientation	Final phase after relaxation	γ^{int} (eV/Å^2)	J^{int} (J/m^2)	A^{int} (pJ/m)
MnBi/Fe_3Co_5		Bi-Co	(111)	crystalline	0.137	0.129	5.4
MnBi/Fe_3Co_5	7.1%, 0°	Mn-Co	(111)	crystalline	0.180	0.127	5.3
MnBi/Fe_3Co_5		Bi-Co	(111)	amorphous	0.130	0.082	2.9
MnBi/Fe_3Co_5	4.8%, 10.5°	Bi-Co	(110)	crystalline	0.129	0.260	5.9
MnBi/Fe_3Co_5		Bi-Co	(110)	disordered	0.127	0.082	1.9

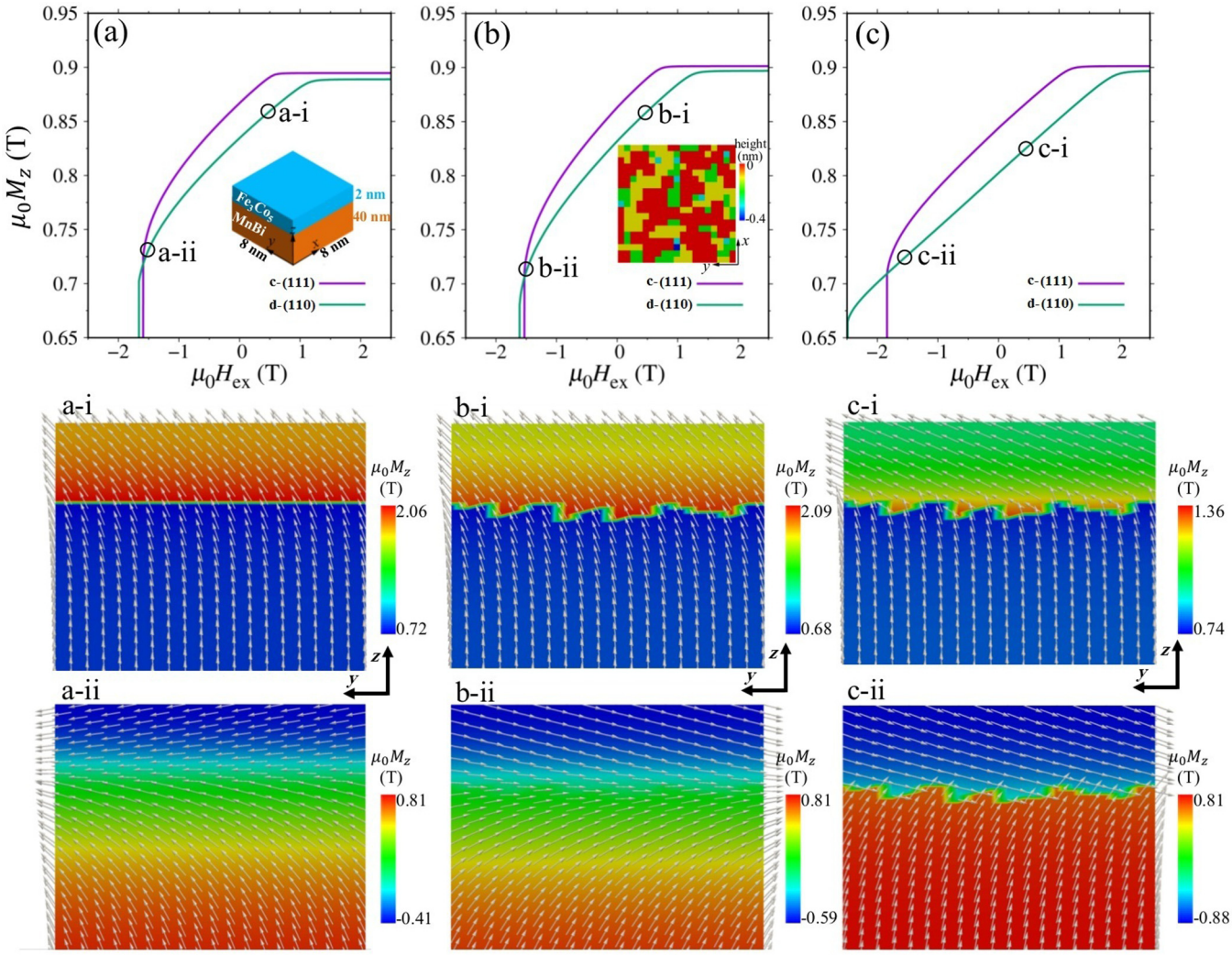

FIG. 4. Micromagnetic simulation results of a MnBi/Fe_3Co_5 model system with disordered FeCo(110) [d-(110)] and crystalline FeCo(111) [c-(111)] interfaces. Magnetic reversal curves: (a) No interface roughness with the A^{int} value listed in Table I. (b) Interface roughness with the same A^{int} as in (a). (c) Interface roughness with A^{int} reduced to 10% of that in (a). The external magnetic field $\mu_0 H_{ex}$ is applied along the z direction. Inset of (a): Model geometry with in-plane periodic boundary condition. Inset of (b): Interfacial roughness of MnBi with a maximum dent height of 0.4 nm. (a-i) and (a-ii), (b-i) and (b-ii), and (c-i) and (c-ii) present the magnetic configurations (yz surface at $x = 0$) corresponding to the marked circles of reversal curves in (a), (b), and (c), respectively, which belongs to the disordered Fe_3Co_5(110).

model based on single crystalline structures to evaluate the exchange behavior. The employed model with an in-plane size of 8×8 nm, 40 nm thick MnBi, and 2 nm thick Fe_3Co_5 is shown in the inset of Fig. 4(a) (including the coordinates). In-plane periodic boundary conditions are applied [16].

Apart from the interface exchange coupling energy, effect of interface roughness and thickness of the soft layer are also evaluated in our micromagnetic simulations [see Figs. 4(b) and 4(c) for the interface roughness and Fig. 5 for thickness analysis of the FeCo layer]. The following cases are considered in Fig. 4.

(i) Perfect flat interface with the interface exchange stiffness of $A^{int}_{(111)} = 5.4$ pJ/m for crystalline Fe_3Co_5 (111) orientation and $A^{int}_{(110)} = 1.9$ pJ/m for disordered Fe_3Co_5 (110) orientation, as shown in Fig. 4(a).

(ii) Rough interface with a random distribution of dent height [maximum 0.4 nm, inset of Fig. 4(b)] in MnBi and the same values of A^{int} as in the case (i), as shown in Fig. 4(b).

(iii) The same rough interface as in the case (ii), but with reduced $A^{int}_{(111)} = 0.54$ pJ/m and $A^{int}_{(110)} = 0.19$ pJ/m, as shown in Fig. 4(c).

It should be noted that the simulated magnetic reversal curves in Fig. 4 do not show the shoulder which was observed in the measured hysteresis loops of the experimental samples. As mentioned earlier, this shoulder could be due to the residual in-plane magnetization component of the hard magnetic phase which was not considered in the micromagnetic simulations but rather assuming a full out-of-plane magnetization vector.

Using micromagnetic simulations we examined the magnetic configuration and its evolution around the interface at different external fields, as shown in the second and third rows of Fig. 4. When the interface is assumed to be perfect and $A^{int}_{(110)} = 1.9$ pJ/m from Table I is used, the magnetization vectors near the interface in FeCo tend to rotate coherently with those in MnBi, as shown in Figs. 4(a-i)

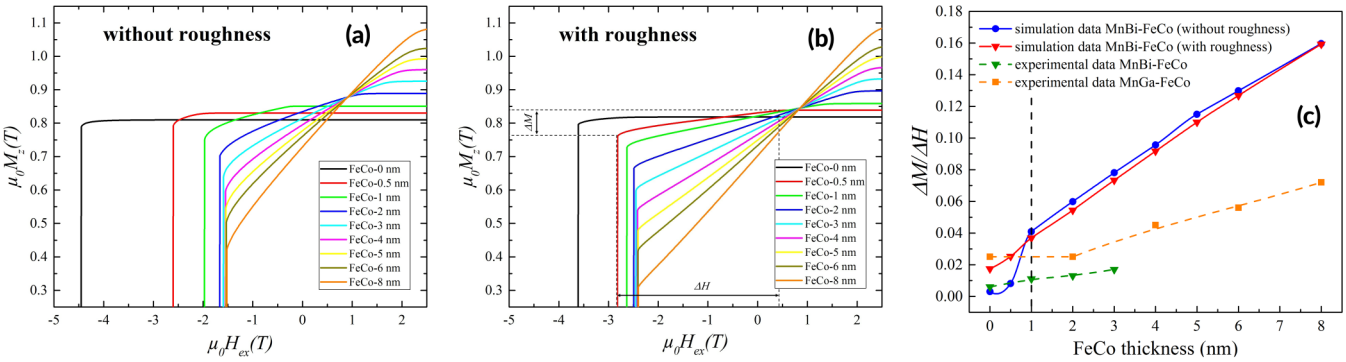

FIG. 5. Hysteresis plots obtained from micromagnetic simulations for MnBi(001)/FeCo(110) double layers (a) without and (b) with interface roughness. (c) Variation of the magnetization with respect to the applied field around zero field for the theoretical and experimental hysteresis plots as a function of FeCo thickness. For the case of interfaces without roughness two regions are evident in which at 1 nm FeCo thickness incoherent coupling between the hard and soft magnetic layers appears. The rough interfaces in both theoretical and experimental cases behave incoherently for all thicknesses. For comparison, the experimental data for the epitaxial case of MnGa(001)/FeCo(001) bilayer are also presented.

and 4(a-ii). This indicates a rather strong interface exchange coupling.

When a rough interface was assumed and $A^{\text{int}}_{(110)}$ was kept the same, Figs. 4(b-i) and 4(b-ii) still suggest strong interface exchange coupling. However, the interface magnetization vectors are much easier to be reversed. This can be verified by comparing the distribution of the z component of magnetization ($\mu_0 M_z$). For instance, at $\mu_0 H_{\text{ex}} = 0.5$ T, the model with rough interface showed a minimum $\mu_0 M_z$ ($\mu_0 M_z^{\text{min}}$) of 0.68 T around the interface [Fig. 4(b-i)], but the model without roughness showed a little higher $\mu_0 M_z^{\text{min}}$ [Fig. 4(a-i)]. The premature reversal in Figs. 4(b-i) and 4(b-ii) could be attributed to the local higher demagnetization field induced by the sharp corners or irregularities in the rough interface [33,34]. Accordingly, the simulated coercivity in Fig. 4(b) was also slightly smaller than that of Fig. 4(a).

When the interface roughness was assumed to reduce $A^{\text{int}}_{(110)}$ to 0.19 pJ/m, the magnetic reversal curve were a simple straight line, as shown in Fig. 4(c). From the magnetic configurations in Figs. 4(c-i) and 4(c-ii), it can also be found that the magnetization vectors around the interface cross each other and the magnetization in FeCo almost rotates freely, indicating a very poor interface exchange coupling.

From Fig. 4 we realize that the interface exchange coupling strength evaluated from DFT calculations of smooth interfaces provides useful insight into atomistic design of the MnBi/FeCo system. In addition, the micromagnetic modeling reveals that the interface roughness and irregular occurrence of defects are also important parameters since it can induce locally premature reversal and, as a consequence, deteriorates the interface exchange coupling.

Figure 5 summarizes the results of thickness analysis based on both experimental measurements and theoretical modeling for MnBi(001)/FeCo(110) interface. In Figs. 5(a) and 5(b), hysteresis plots are shown as a function of FeCo layer thickness for two cases, one without [Fig. 5(a)] and one with interface roughness [Fig. 5(b)], based on the information provided in Fig. 4 for MnBi(001)/disordered Fe_3Co_5(110).

As a descriptor to quantitatively evaluate the changes in degree of exchange coupling caused by interface roughness and increasing soft layer thickness, the first derivative of the corresponding hysteresis loops in Figs. 5(a) and 5(b) (using simulation data) as well as the experimental hysteresis loops in Fig. 2(b) has been calculated. The slope of each hysteresis curve around zero-field crossing, showing the variation of magnetization with respect to the applied field ($\frac{\Delta M}{\Delta H}$), has been also plotted in Fig. 5(c) as a function of FeCo layer thickness. This slope increases with thickness of FeCo layer in both simulation and experiment which implies that the exchange coupling becomes more incoherent and bilayers behave more and more like two separate magnetic layers.

From plots in Fig. 5(c), it can be seen that for structures without interface roughness (blue circles) two regions with different slopes are observable, with a borderline at 1 nm FeCo thickness. It is found that for the sample with less than 1 nm FeCo thickness without interface roughness, the first derivatives are close to zero (the hysteresis loop is more rectangular with slope of ~0), and therefore the hard and soft layers are coherently exchange coupled. However, in case of a rough interface (red triangles) as the slope is continuously increasing the exchange coupling is incoherent regardless of the soft layer thickness.

In addition, the first derivatives of our experimental hysteresis curves for MnBi/FeCo bilayers (green triangles with dashed line) as well as epitaxial MnGa(001)/FeCo(001) bilayers (orange square with dashed line) as a function of FeCo thickness have also been included in Fig. 5(c). As can be seen from the plots in Fig. 5(c), our theoretical and experimental findings for the case of MnBi/FeCo bilayer are in agreement and show that the effect of interface roughness on the incoherency of exchange coupling is significant. Moreover, it can be concluded that the effect of the lattice misfit between the hard and soft layers is decisive since even in the case of the interfaces without roughness (blue solid line) using a single crystalline model, the coherent coupling is only observed up to 1 nm FeCo thickness.

Comparing the trend of derivative plots for MnBi/FeCo and MnGa/FeCo bilayer systems, it can be seen that since MnGa/FeCo bilayers show much decreased interface roughness due to epitaxial growth, a coherent exchange coupling

can be obtained up to 2 nm FeCo thickness. Therefore, it can be concluded that not only interface roughness is limiting the interfacial exchange coupling but also epitaxial growth and a reduced lattice misfit at the interface will greatly improve the coupling behavior.

IV. SUMMARY AND CONCLUSION

In summary, exchange spring MnBi/Fe_xCo_{1-x} ($x = 0.65$ and 0.35) bilayers with different soft magnetic layer thickness were fabricated by dc magnetron sputtering from alloy targets. The magnetic measurements revealed that a Co-rich FeCo soft magnetic layer results in more coherent exchange properties with an optimum soft layer thickness of ∼1 nm leading to ∼3% increase of the saturation magnetization, however, a complete single-phase hysteresis cannot be obtained for higher FeCo thickness. A combined theoretical and experimental approach showed that in the MnBi(001)/FeCo system a combination of crystalline and disordered phases are present close to interface which is expected from the DFT calculations and is also observed in HR-TEM images. The disordered region at the interface considerably limits the exchange coupling effect. As the most important result, micromagnetic simulations showed that the thickness of the soft magnetic layer and the interface roughness between the hard and soft magnetic layers control the effectiveness of exchange coupling. The incomplete exchange coupling observed in MnBi/FeCo bilayers can be correlated with the high interfacial roughness (reducing the exchange constant). Preliminary experimental results show that the MnGa/FeCo epitaxial bilayer has a higher critical soft layer thickness of about 2 nm. Our study suggests that a strong single phase exchange coupling can be extended to higher FeCo thicknesses only through epitaxial growth of both hard and soft magnetic layers with atomically smooth interfaces.

ACKNOWLEDGMENTS

The authors thank the LOEWE project RESPONSE funded by the Ministry of Higher Education, Research and the Arts (HMWK) of the state of Hessen, Germany. We also acknowledge the computing time by the high performance computer center of Hessen (Lichtenberg), and K. Albe from Technische Universität Darmstadt.

[1] N. Poudyal and J. P. Liu, Advances in nanostructured permanent magnets research, J. Phys. D Appl. Phys. **46**, 043001 (2012).

[2] M. J. Kramer, R. W. McCallum, I. A. Anderson, and S. Constantinides, Prospects for non-rare earth permanent magnets for traction motors and generators, JOM **64**, 752 (2012).

[3] D. Li, D. Pan, S. Li, and Z. Zhang, Recent developments of rare-earth-free hard-magnetic materials, Sci. China Phys. Mech. **59**, 617501 (2016).

[4] O. Gutfleisch, M. A. Willard, E. Brück, C. H. Chen, S. G. Sankar, and J. P. Liu, Magnetic materials and devices for the 21st century: Stronger, lighter, and more energy efficient, Adv. Mater. **23**, 821 (2010).

[5] S. Sabet, E. Hildebrandt, F. M. Römer, I. Radulov, H. Zhang, M. Farle, and L. Alff, Low-Temperature phase c-axis oriented manganese bismuth thin films with high anisotropy grown from an alloy $Mn_{55}Bi_{45}$ target, IEEE Trans. Magn. **53**, 2100306 (2017).

[6] J. Park, Y.-K. Hong, J. Lee, W. Lee, S.-G. Kim, and C.-J. Choi, Electronic structure and maximum energy product of MnBi, Metals **4**, 455 (2014).

[7] T. Suzuki, T. Hozumi, J. Barker, S. Okatov, O. Mryasov, and T. Suwa, Investigation into magnetic anisotropy of low-temperature phase MnBi thin films, IEEE Trans. Magn. **51**, 2102804 (2015).

[8] C. Guillaud, Polymorphisme du composé défini MnBi aux températures de disparition et de réapparition de l'aimantation spontanée, J. Phys. Radium **12**, 143 (1951).

[9] E. F. Kneller and R. Hawig, The exchange-spring magnet: A new material principle for permanent magnets, IEEE Trans. Magn. **27**, 3588 (1991).

[10] E. E. Fullerton, J. S. Jiang, M. Grimsditch, C. H. Sowers, and S. D. Bader, Exchange-spring behavior in epitaxial hard/soft magnetic bilayers, Phys. Rev. B **58**, 12193 (1998).

[11] E. E. Fullerton, J. S. Jiang, and S. D. Bader, Hard/soft magnetic heterostructures: Model exchange-spring magnets, J. Magn. Magn. Mater. **200**, 392 (1999).

[12] T. Leineweber and H. Kronmüller, Micromagnetic examination of exchange coupled ferromagnetic nanolayers, J. Magn. Magn. Mater. **176**, 145 (1997).

[13] R. Skomski and J. M. D. Coey, Giant energy product in nanostructured two-phase magnets, Phys. Rev. B **48**, 15812 (1993).

[14] R. Skomski, Aligned two-phase magnets: Permanent magnetism of the future? (invited), J. Appl. Phys. **76**, 7059 (1994).

[15] L. H. Lewis and F. Jiménez-Villacorta, Perspectives on permanent magnetic materials for energy conversion and power generation, Metal. Mater. Trans. A. **44**, 2 (2013).

[16] See Supplemental Material at http://link.aps.org/supplemental/10.1103/PhysRevB.98.174440 for additional details on experimental procedure and theoretical calculations.

[17] T. R. Gao, L. Fang, S. Fackler, S. Maruyama, X. H. Zhang, L. L. Wang, T. Rana, P. Manchanda, A. Kashyap, K. Janicka, A. L. Wysocki, A. T. N'Diaye, E. Arenholz, J. A. Borchers, B. J. Kirby, B. B. Maranville, K. W. Sun, M. J. Kramer, V. P. Antropov *et al.*, Large energy product enhancement in perpendicularly coupled MnBi/CoFe magnetic bilayers, Phys. Rev. B **94**, 060411 (2016).

[18] Y. Yan, J. Guo, J. Li, and R. Li, Magnetically exchange coupled MnBi/FeCo thin film composites with enhanced maximum energy products, Mater. Lett. **184**, 13 (2016).

[19] B. Li, W. Liu, X. G. Zhao, W. J. Gong, X. T. Zhao, H. L. Wang, D. Kim, C. J. Choi, and Z. D. Zhang, The structural and magnetic properties of MnBi and exchange coupled MnBi/Fe films, J. Magn. Magn. Mater. **372**, 12 (2014).

[20] S. Sabet, E. Hildebrandt, and L. Alff, Synthesis and magnetic properties of the thin film exchange spring system of MnBi/FeCo, J. Phys. Conf. Ser. **903**, 012032 (2017).

[21] R. Skomski, P. Manchanda, P. Kumar, B. Balamurugan, A. Kashyap, and D. J. Sellmyer, Predicting the future of permanent-magnet materials, IEEE Trans. Magn. **49**, 3215 (2013).

[22] G. Kresse and J. Furthmüller, Efficient iterative schemes for *ab initio* total-energy calculations using a plane-wave basis set, Phys. Rev. B **54**, 11169 (1996).

[23] J. P. Perdew, K. Burke, and M. Ernzerhof, Generalized Gradient Approximation Made Simple, Phys. Rev. Lett. **77**, 3865 (1996).

[24] V. P. Antropov, V. N. Antonov, L. V. Bekenov, A. Kutepov, and G. Kotliar, Magnetic anisotropic effects and electronic correlations in MnBi ferromagnet, Phys. Rev. B **90**, 054404 (2014).

[25] M. J. Donahue and D. G. Porter, Oommf Software Package, 2016.

[26] C. Kuhrt and L. Schultz, Formation and magnetic properties of nanocrystalline mechanically alloyed Fe-Co and Fe-Ni, J. Appl. Phys. **73**, 6588 (1993).

[27] T. H. Rana, P. Manchanda, B. Balamurugan, A. Kashyap, T. R. Gao, I. Takeuchi, J. Cun, S. Biswas, R. F. Sabirianov, D. J. Sellmyer, and R. Skomski, Micromagnetism of MnBi:FeCo thin films, J. Phys. D Appl. Phys. **49**, 075003 (2016).

[28] N. Umetsu, A. Sakuma, and Y. Toga, First-principles study of interface magnetic structure in $Nd_2Fe_{14}B$/(Fe, Co) exchange spring magnets, Phys. Rev. B **93**, 014408 (2016).

[29] Y. Toga, H. Moriya, H. Tsuchiura, and A. Sakuma, First principles study on interfacial electronic structures in exchange-spring magnets, J. Phys. Conf. Ser. **266**, 012046 (2011).

[30] K. Momma and F. Izumi, VESTA 3 for three-dimensional visualization of crystal, volumetric and morphology data, J. Appl. Crystallogr. **44**, 1272 (2011).

[31] C. Kittel, *Introduction to Solid State Physics*, 8th ed. (Wiley, New Jersey, 2005).

[32] R. Skomski, Nanomagnetics, J. Phys. Condens. Matter. **15**, R841 (2003).

[33] M. Yi, O. Gutfleisch, and B.-X. Xu, Micromagnetic simulations on the grain shape effect in Nd-Fe-B magnets, J. Appl. Phys. **120**, 033903 (2016).

[34] M. Yi, H. Zhang, O. Gutfleisch, and B.-X. Xu, Multiscale Examination of Strain Effects in Nd-Fe-B Permanent Magnets, Phys. Rev. Appl. **8**, 014011 (2017).